



HAL
open science

Surface heat flow and the mantle contribution on the margins of Australia

Bruno Goutorbe, Francis Lucazeau, Alain Bonneville

► **To cite this version:**

Bruno Goutorbe, Francis Lucazeau, Alain Bonneville. Surface heat flow and the mantle contribution on the margins of Australia. *Geochemistry, Geophysics, Geosystems*, 2008, 9 (5), pp.n/a-n/a. 10.1029/2007GC001924 . insu-02933223

HAL Id: insu-02933223

<https://insu.hal.science/insu-02933223>

Submitted on 12 Mar 2021

HAL is a multi-disciplinary open access archive for the deposit and dissemination of scientific research documents, whether they are published or not. The documents may come from teaching and research institutions in France or abroad, or from public or private research centers.

L'archive ouverte pluridisciplinaire **HAL**, est destinée au dépôt et à la diffusion de documents scientifiques de niveau recherche, publiés ou non, émanant des établissements d'enseignement et de recherche français ou étrangers, des laboratoires publics ou privés.



Surface heat flow and the mantle contribution on the margins of Australia

Bruno Goutorbe, Francis Lucazeau, and Alain Bonneville

Équipe de Géosciences Marines, Institut de Physique du Globe de Paris, 4 place Jussieu, F-75252 Paris CEDEX 05, France (goutorbe@ipgp.jussieu.fr)

[1] We present thermal data from 473 oil exploration wells in Australia and New Zealand. Approximately 2300 bottom-hole temperatures are corrected to form a homogeneous set along with 86 temperatures from reservoir tests. Thermal conductivity profiles are estimated from a set of geophysical well logs using a recently developed neural network approach. Retaining wells in which temperature and thermal conductivity data overlap over an interval greater than 1000 m, we estimate 10 heat flow values in the Taranaki basin of New Zealand and 270 values in the northwestern, western, and southern margins and in the intracontinental Canning basin of Australia. The values are in the range 30–80 mW m⁻². As a result of several differences in the data and methods, our heat flow values are 10–20 mW m⁻² lower compared to previously published estimates for the same wells in New Zealand. For Australia, our values are consistent with previously measured values and trends in the continental and marine regions. On the northwestern and southeastern margins, we interpret the variations as reflecting changes in the nature of the underlying basement. Consistent with onshore data, it is inferred that the Archean crust is depleted in radiogenic elements compared to Proterozoic regions and that recent volcanism affects the eastern Paleozoic area. After removing from surface heat flow the sediment contributions, including a permanent radiogenic heat component and a transient sedimentation effect, a simple crustal model suggests that mantle heat flow on the continental margin bordering the Pilbara craton is higher than below the craton itself. Moreover, heat flow corrected for the sediment contributions is markedly lower in the Petrel intracontinental basin than in the adjacent margin, although the crust is thinner below this latter region. As both are underlain by the same basement, this observation may indicate that the mantle contribution is also higher below that margin. Such a higher mantle heat flow on old continental margins is consistent with experiments of fluid convection below an insulating lid and suggests that the thermal regime of the continental lithosphere never returns to its prerift state, as usually assumed by several thermomechanical models of evolution of continental margins.

Components: 7305 words, 10 figures, 2 tables.

Keywords: heat flow; thermal regime; Australia; oil exploration data.

Index Terms: 8130 Tectonophysics: Heat generation and transport; 8105 Tectonophysics: Continental margins: divergent (1212, 8124); 9330 Geographic Location: Australia.

Received 7 December 2007; **Revised** 4 March 2008; **Accepted** 17 March 2008; **Published** 15 May 2008.

Goutorbe, B., F. Lucazeau, and A. Bonneville (2008), Surface heat flow and the mantle contribution on the margins of Australia, *Geochem. Geophys. Geosyst.*, 9, Q05011, doi:10.1029/2007GC001924.

1. Introduction

[2] The thermal regime of the Australian interior is commonly interpreted as the superposition of variable crustal sources, including crustal radiogenic heat and magmatic heat sources, and uniformly low mantle component [Sass and Lachenbruch, 1979; O'Neill et al., 2003]. Few studies tried to extend continental trends toward the continental margins. Therefore, interesting questions related to the thermal regime of the margins and their relation with the continent remain. First, it is worth verifying whether variations of the crustal contribution with respect to crustal age and type are similar to those of the continent's interior. This is not easy, as the nature of basement is poorly constrained on the margins. Second, classical models of evolution for continental margins assume that the lithosphere cools and thickens passively toward its initial state after the extension and breakup phases [e.g., McKenzie, 1978; Voorhoeve and Houseman, 1988]. As a result, the mantle heat flow on old margins should be as low as on the adjacent continent. However, experiments of fluid convection involving an insulating lid conversely suggest that the mantle component increases at the border of the continent [Guillou and Jaupart, 1995].

[3] We had the opportunity to verify these ideas by interpreting oil exploration data in several Australian continental margins, as well as in some intra-continental basins and in the Taranaki basin of New Zealand. After a short description of the tectonic setting and heat flow trends, we describe in the next sections the methodology of heat flow estimation and the interpretation of the results.

1.1. Tectonic Setting

[4] The age of formation of the Australian basement increases roughly from east to west (Figure 1). The westernmost part mainly consists of two Archean cratons, the Pilbara and the Yilgarn, which are surrounded by various Proterozoic mobile belts. The central domain is dominated by Proterozoic belts and Late Archean-Proterozoic blocks. The Gawler craton (Late Archean) and the North Australian craton (an assembly of Archean and Proterozoic units) are located respectively in the southern and northern parts of that area. All these Archean and Proterozoic units, which form the western two-thirds of the continent, were assembled during various orogens until the end of the Proterozoic. The easternmost part of Australia is a Paleozoic feature that originated in a back arc

context related to the subduction of the Pacific plate under the Australian plate, and experienced widespread Cenozoic volcanism [Sutherland, 1978]. To the east, New Zealand is an insular arc also formed as a result of the aforementioned subduction process.

[5] Australian basins experienced tectonic activity during the whole Phanerozoic. To the north, the onshore Canning basin and the Petrel subbasin (of the Bonaparte basin) are the results of failed intra-continental rifts. The former underwent episodes of extension and compression from the Early Ordovician (~500 Ma) to the Early Jurassic (~200 Ma). The latter, which belongs together with the Vulcan subbasin to the Bonaparte basin, was formed during Late Devonian–Early Carboniferous NE–SW extension (~360 Ma). It was subsequently overprinted by major orthogonal rifting events that led to the creation of the northwestern margin basins (Vulcan, Browse, offshore Canning and northern Carnarvon), and culminated in the Middle–Late Jurassic ocean opening in the Timor Sea (~160 Ma) [AGSO North West Shelf Study Group, 1994]. Reactivation occurred during the Late Miocene, as a result of a collision between the Eurasian and Australian plates, and subduction of the latter under Asia at the level of the Banda arc and Timor Island. The Australian western margin is almost exclusively covered by the Perth basin, which resulted from the rifting during the Permian and breakup of Australia and India during the Valanginian [Song and Cawood, 2000]. It is separated from the Yilgarn craton in the east by the Phanerozoic Darling fault system. To the south, rifting between Australia and Antarctica began in the Middle to Late Jurassic (~160–150 Ma) in the Bight basin, and in the Late Jurassic (~140 Ma) in the Otway and Gippsland basins. A Turonian rifting episode in the latter basins stepped out south of the eastern Otway basin leaving the Bass Strait as a failed rift. The Spencer and Tasman fracture zones developed as a result of this irregular rifting geometry. Owing to initial slow spreading rates, the exact time of ocean opening is not precisely known but it seems that the oldest oceanic crust formed around 83 Ma near the Bight basin, and at 44–35 Ma near the Otway basin [Miller et al., 2002], following continental breakup in the interval 95–43 Ma [Finlayson et al., 1998].

1.2. Heat Flow in Australia

[6] Cull [1982] compiled 109 heat flow values on the Australian continent, that globally define three

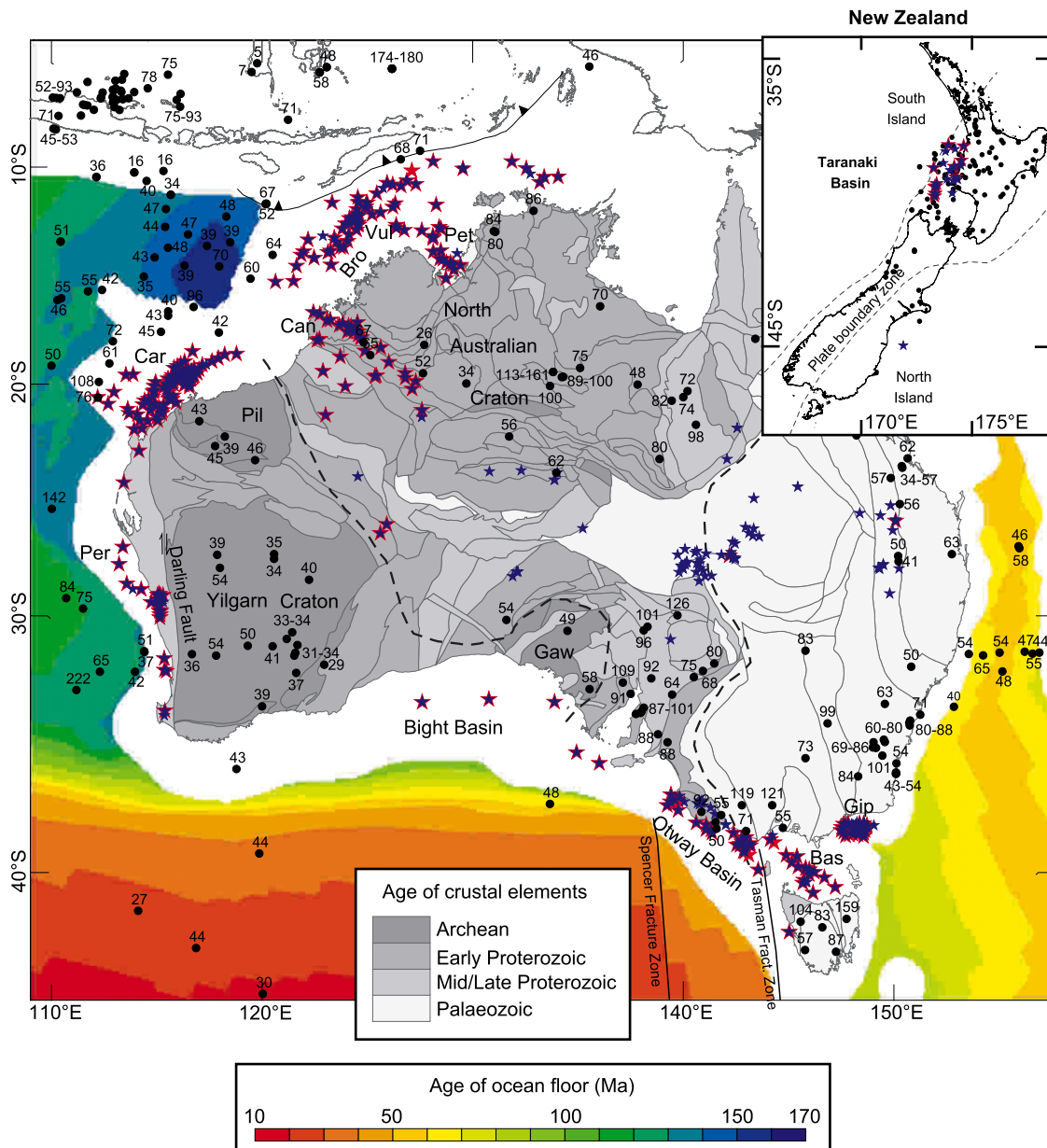


Figure 1. Heat flow data in Australia and New Zealand (not the same scale). Dots: published values, compiled by Cull [1982] in Australia, from Studt and Thompson [1969]; Pandey [1981]; Funnell *et al.* [1996] in New Zealand, and extracted from the global compilation of Pollack *et al.* [1991] completed with more recent ODP values of Pribnow *et al.* [2000] in marine domain. Stars: oil exploration wells used in this study, with well logs (blue stars) and with DST or corrected BHT (red stars). Solid lines delimit the Australian crustal elements [Shaw *et al.*, 1996]. Dashed lines in Australia indicate divisions of major heat flow provinces [Neumann *et al.*, 2000]. Age of ocean floor is from Müller *et al.* [1997] (digital data available on ftp site ftp://ftp.es.usyd.edu.au/pub/agegrid/). Bas, Bass Strait; Bro, Browse basin; Can, Canning basin; Car, Carnarvon basin; Gaw, Gawler Craton; Gip, Gippsland basin; Pil, Pilbara Craton; Per, Perth basin; Pet, Petrel subbasin; Vul, Vulcan subbasin.

heat flow provinces [Sass and Lachenbruch, 1979; Neumann *et al.*, 2000] (Figure 1). Measurements in the western province were performed on the Archean cratons (the Pilbara, the Yilgarn and the Gawler) and define an average of $41 \pm 8 \text{ mW m}^{-2}$

(one standard deviation, 23 values). This low value is consistent with other Archean cratons [e.g., Jaupart and Mareschal, 1999]. The central part of Australia corresponds to a Proterozoic orogen, characterized by extremely large and variable heat

flow values ($80 \pm 24 \text{ mW m}^{-2}$, 46 values). *Sass and Lachenbruch* [1979] interpreted the variations of heat flow in the Archean and Proterozoic domains as the result of crustal heat production variations. A mechanism of heat diversion owing to change of lithospheric thickness, as proposed in southern Africa by *Ballard and Pollack* [1987], is unlikely to explain the Australian pattern observed as the thickest parts of the lithosphere seem to be located below the Proterozoic belts [*Simons et al.*, 1999]. Values on the eastern province are also elevated ($73 \pm 25 \text{ mW m}^{-2}$, 40 values), probably as a consequence of thermal perturbations due to recent (Cenozoic) volcanism [*Sutherland*, 1978].

[7] Using a simple crustal model, *Bodorkos et al.* [2004] proposed that the mantle heat flow is in the range $10\text{--}15 \text{ mW m}^{-2}$ below the Pilbara craton, which is consistent with estimates in other Precambrian shields [*Jaupart and Mareschal*, 1999]. *Sass and Lachenbruch* [1979] found that the reduced heat flow is uniform throughout the continent, and concluded that the surface variations originate solely from the upper crust.

2. Oil Exploration Data Processing

[8] Geophysical well logs and temperature data were obtained from the Wiltshire Geological Services[®] company for 473 oil exploration wells (Figure 1). As no direct measurement of thermal conductivity was available, we estimated it from a set of five geophysical well logs (sonic, density, neutron, electrical resistivity and gamma-ray) using a neural network technique described by *Goutorbe et al.* [2006], in boreholes where all these well logs were recorded. This method was calibrated with data from the Ocean Drilling Program and from STATOIL[®]. The methodology is the same as in a previous study on the South African margins [*Goutorbe et al.*, 2007b]; if needed, thermal conductivity profiles were completed toward the surface assuming that the variations were controlled by porosity. Mean conductivity values are reported in auxiliary material¹ Data Set S1.

[9] Two types of temperatures were used: 86 stationary fluid temperatures acquired during drill-stem tests (DST), and about 2300 bottom-hole temperatures (BHT) measured during logging phases. DST are measured during reservoir testings on formation fluids that flow to the surface through the drill-pipe, inflatable packers being used to

isolate the section of the borehole to be tested. It is assumed that the fluids are in equilibrium with the surrounding rocks, so that DST are considered as most representative of formation temperatures [*Perrier and Raiga-Clemenceau*, 1984]. BHT are usually recorded using a maximum recording thermometer attached to the geophysical logging tool. They are perturbed because of the effect of drilling and mud circulation, but it is possible to extrapolate the true formation temperature from a time series of BHT measured at a given depth after the end of mud circulation. After a review of the correction methods that can be used to perform such an extrapolation (described by *Goutorbe et al.* [2007a]), we chose to apply the correction developed by *Middleton* [1982], in which it is assumed that the perturbation acts as an instantaneous sink of heat, so that:

$$T_{\text{BHT}}(t_e) = T_{\infty} - \Delta T \cdot \left[1 - \exp\left(-\frac{r^2}{4\kappa t_e}\right) \right], \quad (1)$$

where T_{BHT} is a BHT measurement, t_e the elapsed time after the end of mud circulation, T_{∞} the true formation temperature, ΔT the initial difference of temperature between the borehole and surrounding rocks, r the borehole radius and κ the thermal diffusivity of rocks. t_e is usually given along with T_{BHT} and r can be deduced from the caliper log. The thermal conductivity λ and the neutron log ϕ are used to obtain an estimation of κ :

$$\kappa = \frac{\lambda}{\phi \rho c_w(T) + (1 - \phi) \rho c_m(T)}, \quad (2)$$

where $\rho c_w(T)$ and $\rho c_m(T)$ are, respectively, the volume heat capacity of water and rock matrix, depending on temperature T . $\rho c_m(T)$, which hardly varies from one rock type to another, is inferred from *Vosteen and Schellschmidt* [2003] and $\rho c_w(T)$ from *Lide* [2004]. The in situ temperature T is roughly estimated from DST measurements. T_{∞} and ΔT being a priori unknown, one needs a time series of at least two BHT measurements in order to extrapolate T_{∞} . From the data set it was possible to build up about 650 time series of BHT measurements, on which were performed least-square adjustments using equation (1) in order to deduce T_{∞} and ΔT corresponding to each of them. In boreholes containing both types of measurements, the corrected temperatures T_{∞} are in good agreement with DST [*Goutorbe et al.*, 2007a].

[10] The usual procedure is then to fit the ΔT obtained in this way as a function of depth z , so

¹Auxiliary materials are available at <ftp://ftp.agu.org/apend/gc/2007gc001924>.

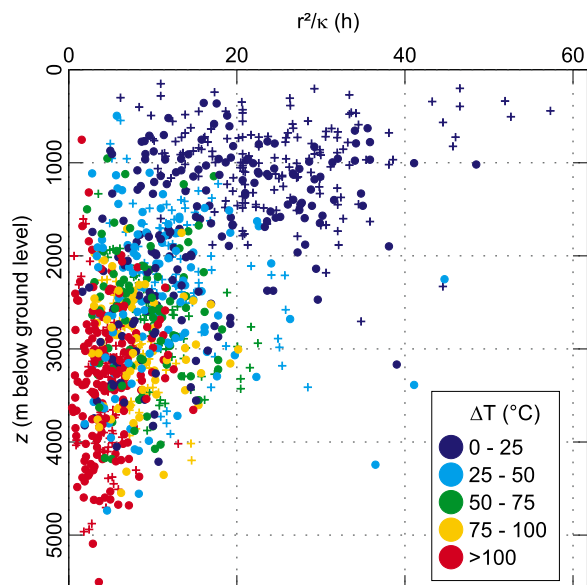


Figure 2. Dots: ΔT obtained by correcting time series of BHT measurements, versus z and r^2/κ . Crosses: ΔT deduced for single measurements by performing a moving average in the $(z, r^2/\kappa)$ space (see text for details).

as to allow one to extrapolate T_∞ from the remaining single BHT data that do not belong to any time series (about 300 in our case). The idea of this so-called “depth-time” correction, proposed by *Deming and Chapman* [1988], is that there is a weak relationship between the unknown correction factor (ΔT in our case) and depth z reflecting the increasing contrast between the mud and surrounding rocks temperature as great depths are reached. We assumed that the perturbation is also likely to depend on rocks thermal properties and borehole radius, and therefore we decided to fit ΔT as a function of both z and r^2/κ . Indeed, the correlation is significantly better with both variables taken into account than with only z (Figure 2). ΔT was fitted to z and r^2/κ by performing a moving average, using a search ellipse of radii $R_{r^2/\kappa} = 10^4$ s (≈ 3.8 h) along the r^2/κ -axis and $R_z = 250$ m along the z -axis. The radii were extended to $R_{r^2/\kappa} = 4 \cdot 10^4$ s (≈ 11.1 h) and $R_z = 1000$ m if no data could be found within the previous search ellipse to perform the moving average (which occurs mainly at small depths; see Figure 2).

[11] In order to constrain thermal gradients over large intervals, we assigned a ground temperature to each borehole. It was inferred from the worldwide ocean temperature profiles of *Levitus and*

Boyer [1994] for offshore wells, and from a global climate database compiled by *Leemans and Cramer* [1991] for onshore wells (updated in 1996 and available at <http://www.pik-potsdam.de/members/cramer/climate.html>). The different types of temperature (DST, corrected multiple BHT, corrected single BHT, ground temperature) form a globally homogeneous temperature set (Figure 3). Ground temperatures and average thermal gradients are reported in auxiliary material Data Set S1.

[12] We applied the inversion scheme of *Vasseur et al.* [1985] in order to compute heat flow values, under the assumptions of (1) stationary and conductive heat transfer and (2) correlation of the errors on thermal conductivity. It is essential to introduce the last point into the inversion procedure; indeed, if the estimates of thermal conductivity at successive depths are considered to be uncorrelated variables, the dense sampling leads the inversion to consider the profile as a whole as

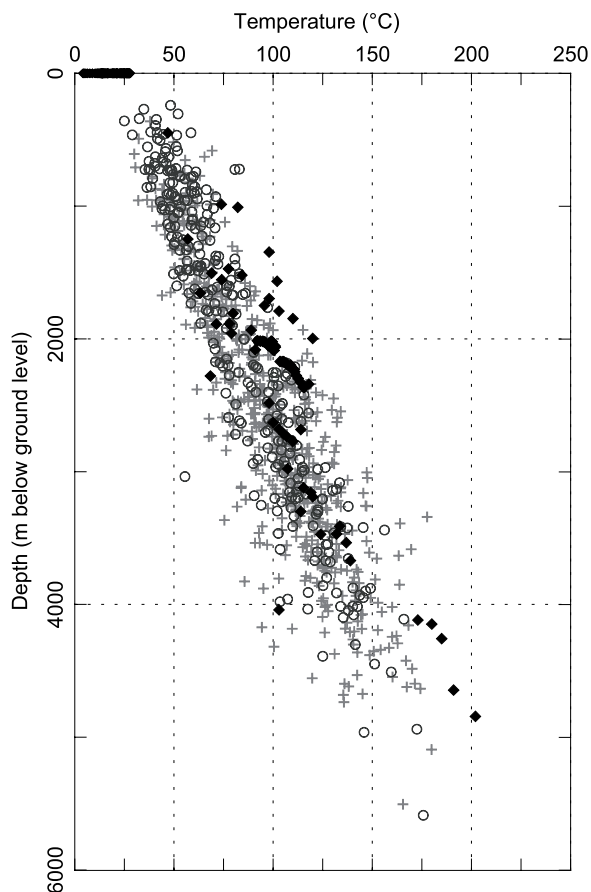


Figure 3. Temperature versus depth. Black diamonds, DST and ground temperatures; grey crosses, corrected multiple BHT; open circles, corrected single BHT.

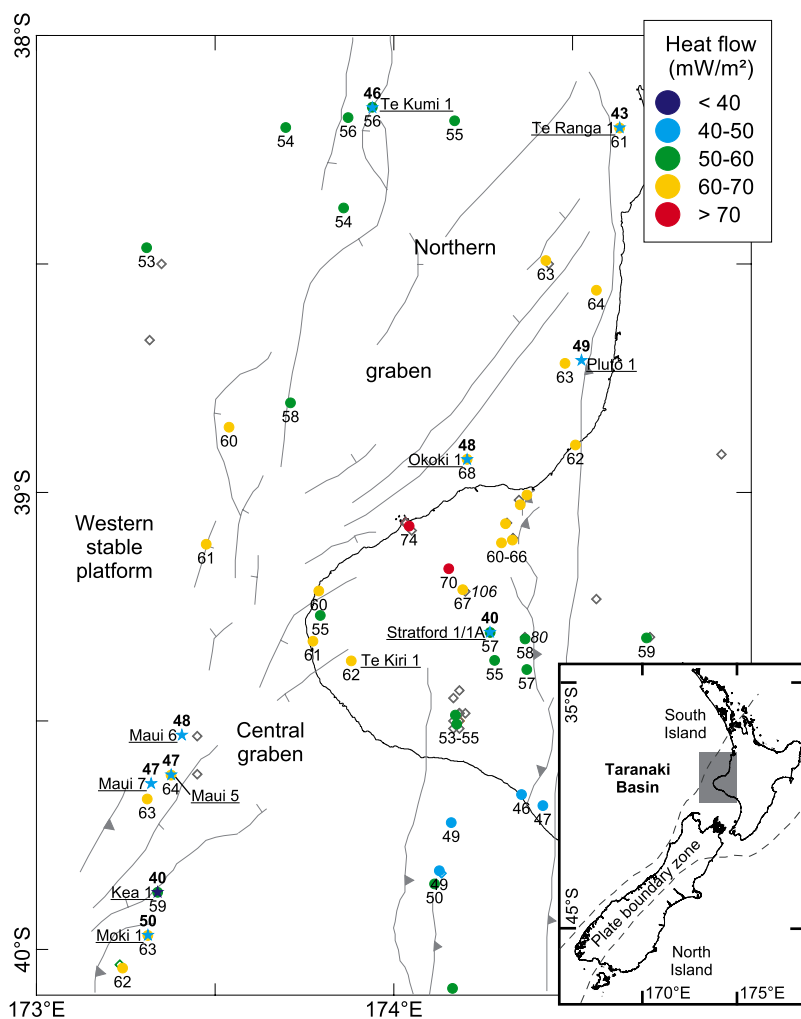


Figure 4. Heat flow results in New Zealand. Dots with normal labels underneath: values from *Funnell et al.* [1996]. Stars with bold labels above: values from this Study. Underlined labels: name of the wells of this study. Major structural features are from *Funnell et al.* [1996]. Locations of the data from *Pandey* [1981] are shown as grey diamonds, but the corresponding heat flow values are not reported as they are likely to be overestimated (see text for details).

completely accurate, which implies a total control of thermal conductivity on the a posteriori geotherm, and underestimation of the a posteriori uncertainty on heat flow.

[13] The contribution of sediments could also be estimated in part of the wells. This contribution comprises two components, namely, the heat brought by the radiogenic elements contained in the sediments (say, Q_{r_s}) and the transient reduction due to the sedimentation process itself (say, Q_s). In order to estimate Q_{r_s} , we calculated heat production A in every well in which spectral gamma ray log was available, using the relation of *Bücker and Rybach* [1996]. Then, the average \bar{A} was assigned

to each basin. Finally, we assumed that radiogenic elements were uniformly distributed within the sediments, so that for every well of a basin, $Q_{r_s} = \bar{A} \cdot d$, with d the sediment thickness at well location, estimated from EXXON maps [*Kaplan et al.*, 1985]. We computed Q_s from lithostratigraphic descriptions, using the numerical model of *Lucazeau and Le Douaran* [1985]. Heat flow corrected for the sediment contributions Q_{corr} can be deduced from the raw value Q :

$$Q_{\text{corr}} = Q - Q_{r_s} + Q_s \quad (3)$$

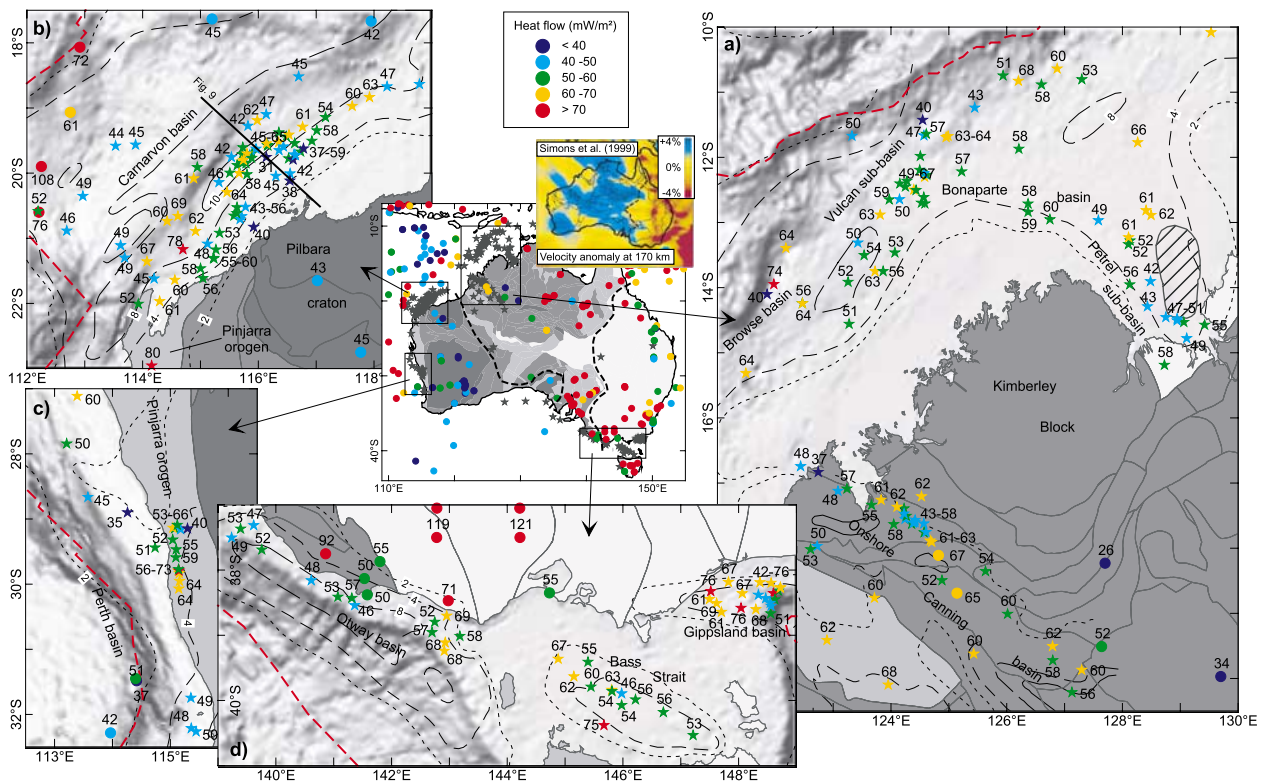


Figure 5. Heat flow results in Australia. Dots: previously published values. Stars: values from this study. Short dashed to solid lines: 2, 4, 8, and 10 km sediment isopachs. Shaded relief maps: offshore topography. Red dashed line: ocean-continent transition [after Müller *et al.*, 1997]. Tectonic elements (light grey to dark grey areas) and heat flow provinces (delimited by thick dashed lines) are similar to Figure 1. In the Petrel subbasin (Figure 5a), the hatched area is the location of the gravity anomaly (>20 mGal). In the Carnarvon basin (Figure 5b), the thick line corresponds to the profiles in Figure 9. Note that some values from this study are outside the zoomed areas. The inset at the top right of the central map shows a slice at 170 km depth of the shear wave speed model of Simons *et al.* [1999].

Results are reported in auxiliary material Data Set S1 and in Figures 4 and 5 and are discussed in the following section.

3. Results and Discussion

3.1. Data Description

[14] There are 10 rather homogeneous estimates in the Taranaki basin of New Zealand between 40 and 50 mW m^{-2} (Figure 4), which yield a low average of 46 ± 4 mW m^{-2} (one standard deviation). In Australia we computed 270 values, mostly distributed in the northwestern, western and southeastern margins (Figure 5), which are in the range 30–80 mW m^{-2} . Heat flow in the central southern region of the Petrel basin is low (49 ± 5 mW m^{-2} , 9 values) and increases toward the northern region to 50–60 mW m^{-2} (Figure 5a). For basins of the western area of the northwestern continental mar-

gin (Browse, Vulcan, northern Bonaparte basins), the range is 50–65 mW m^{-2} , except for a few low values near the subduction zone. The trend of the onshore Canning basin is complex, with heat flow in the range 50–65 mW m^{-2} in the southeastern region, and a high variability near the coastline (30–60 mW m^{-2}) (Figure 5a). In the Carnarvon basin (eastern part of the northwestern margin), the lowest estimates are found near the coastline in front of the Pilbara Archean craton (38–45 mW m^{-2}), while markedly higher values, around 60–70 mW m^{-2} , are encountered in the vicinity of the Proterozoic regions (Figure 5b). Some data suggest that heat flow tends to be low (45–50 mW m^{-2}) toward the oceanic domain. In the Perth basin (western margin), offshore data are almost 10 mW m^{-2} lower than onshore values: 48 ± 7 mW m^{-2} (8 values) versus 58 ± 9 mW m^{-2} (14 values) (Figure 5c). Finally, on the southeastern margin, the Otway basin shows two distinct styles

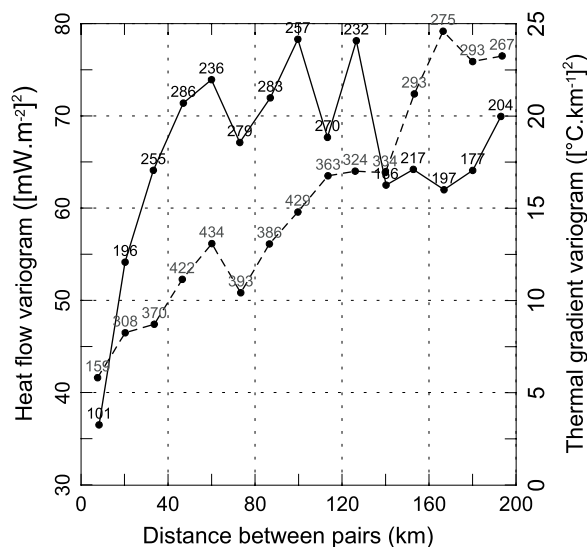


Figure 6. Experimental variograms of thermal gradient (dashed line and dots) and heat flow (solid line and dots) from this study. Numbers indicate the number of pairs at each point.

in the vicinity of the onshore Proterozoic and Paleozoic domains (as defined by *Shaw et al.* [1996]); in front of the former there is an average of $51 \pm 4 \text{ mW m}^{-2}$ (8 values), while mean heat flow reaches $62 \pm 7 \text{ mW m}^{-2}$ (6 values) near the latter (Figure 5d). In the Bass Strait, most values homogeneously fall in the range $55\text{--}60 \text{ mW m}^{-2}$. Heat flow is elevated in the Gippsland basin, where data range between 60 and 80 mW m^{-2} , except for a cold region toward the oceanic domain where values are $<55 \text{ mW m}^{-2}$.

[15] It should be noted that spatial continuity of thermal gradient and heat flow from this study is satisfied (Figure 6), which indicates that relative variations are not mere noise. Thermal gradient is a quasi-continuous variable of space (its variogram tends to zero as distance approaches zero). Small-scale variability of heat flow is $\sim 35 \text{ [mW m}^{-2}]^2$, that is about 6 mW m^{-2} , which is of the order of heat flow uncertainty (see auxiliary material Data Set S1).

3.2. Comparison With Published Values

[16] *Pandey* [1981] and *Funnell et al.* [1996], using oil exploration data, previously estimated heat flow in the Taranaki basin of New Zealand (Figure 4). They constrained thermal gradients using oil exploration BHT. Regarding thermal conductivity, *Pandey* [1981] used a single value

per borehole, derived from needle-probe measurements on low-porosity cores, while *Funnell et al.* [1996] applied a geometric mixing law to end-members lithologies, whose thermal conductivity was deduced from sample measurements. We will limit the comparison to the latter study, because *Pandey* [1981] did not apply any porosity correction, which is likely to overestimate thermal conductivity values and consequently also heat flow estimates. Heat flow values from *Funnell et al.* [1996] are systematically higher by $10\text{--}20 \text{ mW m}^{-2}$ than ours, which is partly accounted for by differences of $1\text{--}5^\circ\text{C km}^{-1}$ between thermal gradients (Table 1). As the latter effect cannot explain alone heat flow discrepancies, there are obviously differences between thermal conductivity estimates. However, a direct comparison cannot be made because the mean conductivity values are not available from *Funnell et al.* [1996].

[17] The possible causes for differences and their estimated effect are reviewed here:

[18] 1. *Funnell et al.* [1996] used the Bullard line source model [*Bullard*, 1947] with a constant thermal diffusivity $\kappa = 5 \cdot 10^{-7} \text{ m}^2 \text{ s}^{-1}$ in order to correct their BHT; applying the same BHT correction method to our data does not significantly modify the results.

[19] 2. Differences in thermal gradients are reduced by a few $^\circ\text{C km}^{-1}$ by constraining the ground temperature to 10°C ; this lower than the present value was introduced by *Funnell et al.* [1996] to account for the deep paleoclimatic effects related to the rise in temperature 14000 years ago.

Table 1. Comparison of Results From *Funnell et al.* [1996] and Results From This Study

Well Name	This Study		Funnell et al.	
	∇T^a	Q^a	∇T^a	Q^a
Kea 1	26	40 ± 09	29	59 ± 8
Maui 5	31	47 ± 10	33 ^b	64 ± 5
Maui 6	31	48 ± 10		
Maui 7	30	47 ± 10		
Moki 1	27	50 ± 12	31 ^c	63 ± 9
Okoki 1	29	48 ± 14	30	68 ± 6
Stratford 1/1A	26	40 ± 11	26	57 ± 4
Te Kumi 1	26	46 ± 13	31	56 ± 5
Te Ranga 1	24	43 ± 08	29	61 ± 5

^a ∇T , mean thermal gradient ($^\circ\text{C km}^{-1}$); Q , heat flow (mW m^{-2}).

^b This value actually corresponds to Maui 5–7.

^c This value actually corresponds to Moki 1–2.

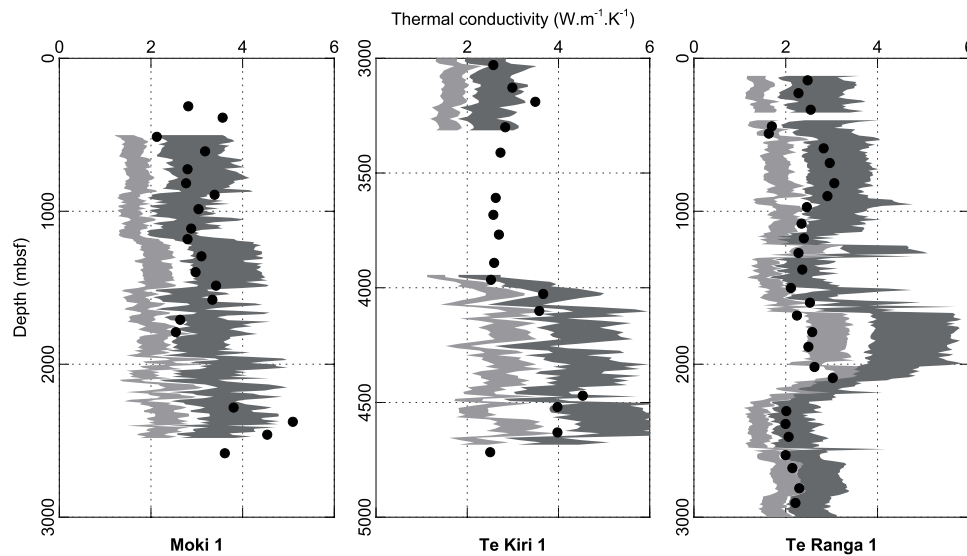


Figure 7. Comparison of matrix thermal conductivity measurements from *Funnell et al.* [1996] and neural network estimates. Light grey: neural network estimates with $\pm 15\%$ uncertainty. Dark grey: corresponding predicted range for matrix thermal conductivity, obtained by (1) estimating porosity from the neutron porosity log, (2) assuming a geometric mixing law model for the rock conductivity (matrix + pore water), and (3) correcting the values from the temperature effect using the *Chapman et al.* [1984] formula in order to reflect laboratory conditions. Dots: matrix thermal conductivity measured by *Funnell et al.* [1996].

[20] 3. However, a residual difference up to 4°C km^{-1} remains for some wells; we presume that it is related to dissimilarities in the raw temperature sets themselves.

[21] 4. *Funnell et al.* [1996] measured the thermal conductivity of some lithologic end-members on cuttings, then applied a geometric multi-components (including pore water) mixing model in order to estimate in situ thermal conductivity. Our estimates from neural networks, replaced in laboratory conditions (i.e., corrected for the porosity and temperature effects), are consistent with their measurements (Figure 7). The differences may arise from porosity, which is derived from sonic logs from *Funnell et al.* [1996] and seems lower than porosity from neutron logs (Figure 8). The presence of shale is known to overestimate the porosity derived from neutron logs [e.g., *Serra and Serra, 2004*] by about 10–15%, but differences between the sonic porosity of *Funnell et al.* [1996] and the neutron porosity still appear for low values of gamma ray, corresponding to nonshaly facies for which the neutron porosity is more likely to be accurate (Figure 8). Thus, the higher thermal conductivity of *Funnell et al.* [1996] may be the result of their low estimated porosity.

[22] In Australia, it is not possible to make a direct comparison to the margins, but our data are globally consistent with regional trends:

[23] 1. In the southeastern part of the onshore Canning basin, there are three published values respectively equal to 52 mW m^{-2} , 65 mW m^{-2} and 67 mW m^{-2} [*Cull, 1982*], in agreement with our

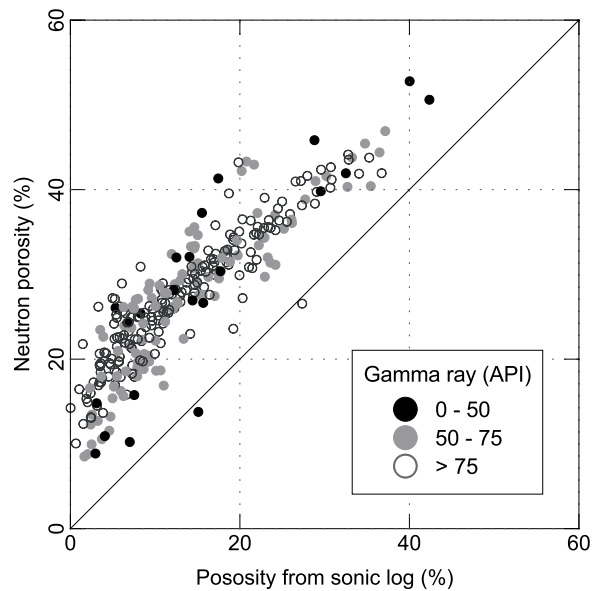


Figure 8. Neutron porosity log versus porosity deduced from sonic log using the same relation as *Funnell et al.* [1996] and *Armstrong et al.* [1998], grouped by classes of gamma ray. Log values were averaged over 100 m intervals. Standard logger unit for gamma ray log is American Petroleum Institute (API) unit.

Table 2. Estimates of Contribution From Sediments Radiogenic Heat Production and Sedimentation Process to Heat Flow by Basin

Basin	\bar{A}^a	\bar{d}^a	\overline{Q}_{rs}^a	\overline{Q}_s^b	\overline{Q}_{corr}^c
Bass	1.4 (2)	4.5 ± 1.5	6.5 ± 2	5.5 ± 2	53 ± 6
Bonaparte	1.4 (29)	5.5 ± 1	7.5 ± 1.5	3.5 ± 2.5	51 ± 8
Petrel subbasin	1.6 (10)	5 ± 1	7.5 ± 2	1.5 ± 0.5	
Central southern					41 ± 5
Northern					49 ± 6
Vulcan subbasin	1.3 (14)	6 ± 0.5	7.5 ± 0.5	5 ± 2.5	52 ± 8
Browse	1.3 (5)	7 ± 1	8.5 ± 1	4.5 ± 3	54 ± 10
Canning (onshore)	1.5 (4)	5 ± 2.5	7.5 ± 4	1 ± 0.5	47 ± 8
Carnarvon	1.4 (30)	8.5 ± 2	11 ± 3	3 ± 2	45 ± 9
High h.f. region ^d	1.4 (12)	7.5 ± 2	10 ± 3	2 ± 1	50 ± 9
Low h.f. region ^d	1.4 (18)	8.5 ± 2	12 ± 3.5	4 ± 2	44 ± 8
Gippsland	1.2 (8)	4.5 ± 1	6 ± 1	13 (one val.)	83 (one val.)
Otway	1.6 (5)				
West (<142°E)		5.5 ± 2	12 ± 1.5		
East (>142°E)		4.5 ± 2	7.5 ± 2.5		
Perth	2.3 (2)				
Offshore		4.5 ± 2.5	10 ± 5.5	1.5 ± 0.5	37 ± 6
Onshore		3 ± 0.5	7 ± 1	1.4 ± 0.1	57 ± 9

^a \bar{A} , mean sediments heat production ($\mu\text{W m}^{-3}$), derived from spectral gamma ray logs (number of wells in parentheses); \bar{d} , mean sediments thickness (km, \pm one s.d.) at wells location, from EXXON maps [Kaplan *et al.*, 1985]; \overline{Q}_{rs} , mean contribution from sediments radiogenic heat production to heat flow (mW m^{-2} , \pm one s.d.); individual wells values are in auxiliary material Data Set S1.

^b \overline{Q}_s , mean heat flow reduction due to sedimentation process (mW m^{-2} , \pm one s.d.), based on lithostratigraphic descriptions and using the numerical model of Lucazeau and Le Douaran [1985]; individual wells values are in auxiliary material Data Set S1.

^c \overline{Q}_{corr} , mean heat flow corrected from the sediment contribution (mW m^{-2} , \pm one s.d.): $Q_{corr} = Q - Q_r + Q_s$, with Q the raw estimate.

^dRegions bordering respectively Proterozoic and Archean continental crust (see Figure 5 and text for details).

estimated heat flow range of 50–65 mW m^{-2} (see section 3.1 and Figure 5a).

[24] 2. In the Carnarvon basin, published offshore data show a high variability (Figure 5b), which makes them difficult to compare with our values. There is a group of high heat flow in the west (61–108 mW m^{-2}); one of them, actually corresponding to ODP site 763A [Pribnow *et al.*, 2000], displays a large difference to an oil exploration well very close by (Vinck 1): 76 mW m^{-2} for the former versus 52 mW m^{-2} for the latter (see Figure 5b, left-hand side). This difference could be due to the smaller depth of measurement of ODP temperatures. On the other hand, values in the north (42 mW m^{-2} and 45 mW m^{-2}) are consistent with our data toward the oceanic domain.

[25] 3. Finally, in the Otway basin, a few continental values close to the coastline are in very good agreement with our marine data, except for a very high estimate of 92 mW m^{-2} : in the western region a continental group ranges 50–55 mW m^{-2} and can be compared to our estimates (46–57 mW m^{-2}); in the eastern region a single continental value of 71 mW m^{-2} is similar to very close marine data yielding 69 mW m^{-2} (Figure 5d).

3.3. Heat Flow and Crustal Sources

[26] Variations of continental surface heat flow in Australia are commonly related to differences in crustal heat production in the Precambrian regions forming the western two-thirds of the continent, and upper crustal magmatic sources in the Paleozoic fold belts forming the remaining third (see section 1.2 and Sass and Lachenbruch [1979]). This section reviews heat flow variations on continental margins that are visibly related to the nature of the underlying crust.

[27] As described in section 3.1, low values (38–45 mW m^{-2}) are observed on the Carnarvon basin at the border of the Archean Pilbara craton, while a region of markedly higher heat flow (60–70 mW m^{-2}) is seen in the vicinity of the Late Proterozoic orogen (Figure 5b). The low values are in agreement with the high seismic velocity anomaly extending toward the ocean (Figure 5) [Simons *et al.*, 1999]. The difference between heat flow values cannot be explained by differences in the sediment contribution, which does not vary significantly (Table 2). They are more likely due to different crustal contributions if we infer that the Late Proterozoic Pinjarra orogen is more enriched in

radiogenic elements than the Archean crust. The latter point is consistent with the trends of heat production in the Precambrian part of the continent, which show that the Archean crust is depleted in radiogenic elements compared to the central Proterozoic regions [Sass and Lachenbruch, 1979]. Moreover, this assumption is corroborated by the high values of the onshore Perth basin overlying the Pinjarra orogen (Figure 5c) defined by an average of $57 \pm 9 \text{ mW m}^{-2}$ (3 values) after removing the sediment contributions (Table 2), while the continental Archean domains yield $41 \pm 8 \text{ mW m}^{-2}$ (4 values).

[28] In the Otway basin (southeastern margin), heat flow increases more than 10 mW m^{-2} between the western and the eastern regions (see section 3.1 and Figure 5d). The radiogenic contribution of the sediments increases this difference (Table 2), but there is no available information to estimate the effect of the sedimentation process. The difference is more likely to be related to crustal sources, because the transition between Proterozoic and Paleozoic crusts, as defined by Shaw *et al.* [1996], corresponds to the changes in surface heat flow.

[29] Finally, recent volcanism probably explains the high values encountered in the Gippsland basin ($60\text{--}70 \text{ mW m}^{-2}$), in which the only sedimentation correction available suggest that more than 10 mW m^{-2} might be added after correction (Table 2). The high values are consistent with the extremely slow wave speeds at the easternmost part of the Paleozoic fold belts (Figure 5) [Simons *et al.*, 1999].

3.4. Mantle Heat Flow on the Northwestern Margin

[30] All continental margins of this study, except for the Otway basin, are of a sufficient age that thermal relaxation of the lithosphere should be now completed (age of continental breakup greater than 90 Ma). Therefore the mantle component on the margins should reflect steady state conditions, and can be compared to that of the continent. In this section such comparisons are made on the northwestern margin of Australia: as its crustal structure was extensively studied, it is possible to make assumptions on the contribution of the crust to surface heat flow and therefore quantify the trends of mantle heat flow.

[31] In the Carnarvon basin, data are located in a 150–250 km wide area from the coastline to the limits of the continental plateau (Figure 5b), with no apparent decreasing heat flow. On the offshore

domain in the vicinity of the Archean craton, heat flow corrected for sediment contributions (i.e., sediment radiogenic heat and sedimentation process) define an average of 43 mW m^{-2} (~ 25 values). These heat flow estimates are comparable to the values of the Archean continental domains of Australia in general and to those of the Pilbara craton in particular (Figure 9). The upper and radiogenic part of the continental crust is significantly thinned in this area [Driscoll and Karner, 1998], which requires that the mantle heat flow is enhanced in order for the surface heat flow to remain constant. Assuming that the nature of the crust is similar to that of the adjacent Archean domain, the upper bound for the heat production of the upper crust can be $2.1 \mu\text{W m}^{-3}$, which is a value representative of granite heat production in the Pilbara craton [Bodorkos *et al.*, 2004]. An average of $0.2 \mu\text{W m}^{-3}$ is assigned to the lower crust, following the global mean of Rudnick and Fountain [1995]. These values yield an upper bound for the crustal contribution to surface heat flow (Figure 9), which can be subtracted from surface heat flow estimates corrected for the sediment contributions in order to deduce a lower bound for the mantle heat flow. Figure 9 shows that the mantle contribution should be at least $20\text{--}30 \text{ mW m}^{-2}$ in order to account for the observations. This is higher than the estimate of $10\text{--}15 \text{ mW m}^{-2}$ for the mantle heat flow below the adjacent Pilbara craton [Bodorkos *et al.*, 2004].

[32] Still on the northwestern margin of Australia, the Browse, Vulcan and Petrel basins are underlain by the same Proterozoic basement that forms the Kimberley Block [Symonds *et al.*, 1994]. Seismic data [Goncharov, 2004] and gravity modeling [Baldwin *et al.*, 2003] suggest that the crust is extremely thinned in the Petrel subbasin (as low as 5 km). Wells from the central southern region of the Petrel subbasin (latitude $> 13.5^\circ\text{S}$) are located outside the gravity anomaly area (Figure 5a), where the crust is 20–25 km thick [Baldwin *et al.*, 2003]. In this region, the average heat flow corrected for sediment contributions is $41 \pm 4 \text{ mW m}^{-2}$ (9 values). On the other hand, wells from the northern part of the Petrel subbasin are located above a 5–10 km thick basement [Baldwin *et al.*, 2003; Goncharov, 2004], where average heat flow is $49 \pm 6 \text{ mW m}^{-2}$ (6 values). Below the Vulcan and Browse basins, seismic studies suggest that the Precambrian basement is uniformly 10–15 km thick [Petkovic *et al.*, 2000; Goncharov, 2004], while average heat flow is $52 \pm 8 \text{ mW m}^{-2}$ (23 values) and 54 ± 10 (14 values) respectively.

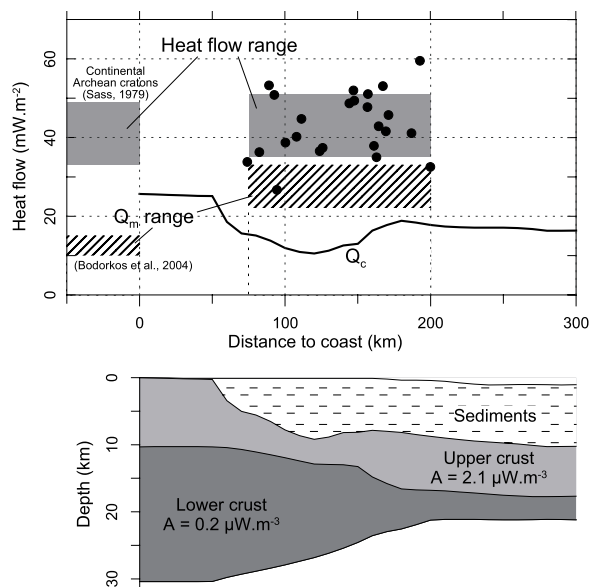


Figure 9. (top) Heat flow versus distance to coast along the line shown in Figure 5b. Dots: values from this study corrected from the sediment contributions, “close enough” to the line shown in Figure 5b (maximum distance = 100 km). Grey areas: range of heat flow values (± 1 s.d.). Hatched areas: estimated range for mantle heat flow Q_m . Crustal contribution Q_c (solid line) is estimated from the model shown at the bottom, assuming that lateral heat conduction is negligible. Continental heat flow values fall outside this figure, but the range for surface and mantle heat flow of Archean domains is shown on the left. (bottom) Crustal section, from *Driscoll and Karner* [1998]. Heat production values A are taken from *Bodorkos et al.* [2004].

These observations show that surface heat flow does not correlate with crustal thickness and that an increase of mantle contribution is needed to explain the oceanward values (Figure 10). Let us assume that the southern central region of the Petrel subbasin is characterized by a continent-like low mantle heat flow, in the range $10\text{--}15\text{ mW m}^{-2}$. Then, making the assumption that crustal radiogenic contribution is linearly related to total crustal thickness, mantle heat flow toward the margin could be as high as $30\text{--}45\text{ mW m}^{-2}$ (Figure 10). The assumption of linear dependence is rough, but not too far from reality if (1) heat production does not vary significantly over the considered area (which is underlain by the same basement) and (2) crustal thinning is homogeneous over the entire crustal section.

[33] Such trends of increasing mantle heat flow toward the continental margins have been previ-

ously observed on the Congo-Angola margin [*Lucazeau et al.*, 2004] and the South African margins [*Goutorbe et al.*, 2007b]. There are also elevated values on the Kenya-Tanzania margin [*Nyblade*, 1997, Figure 3] that could be interpreted in such a way. Moreover, an inspection of heat flow distributions derived from a global seismic model [*Shapiro and Ritzwoller*, 2004] suggests that mean heat flow on old margins can be slightly greater than that of the adjacent continent and even that of the adjacent ocean. The estimates of high mantle heat flow on old continental margins should urge one to reconsider the classical models of evolution of passive margins, which assume that the lithosphere cools passively and tends toward its pre-extension state. In fact, this assumption implies an unrealistic step geometry for continental margins, as continental lithosphere is usually much thicker than its oceanic counterpart. Such a geometry would be obviously unstable within the mantle convection system, and our results indeed suggest that basal heat flow does not tend back to its initial, low continental value. We think that the models could be valid for intracontinental basins, which would explain the low heat flow values in the southern region of the Petrel subbasin, but not for continental margins because of the interaction between the ocean-continent transition and the underlying mantle convection. This is consistent

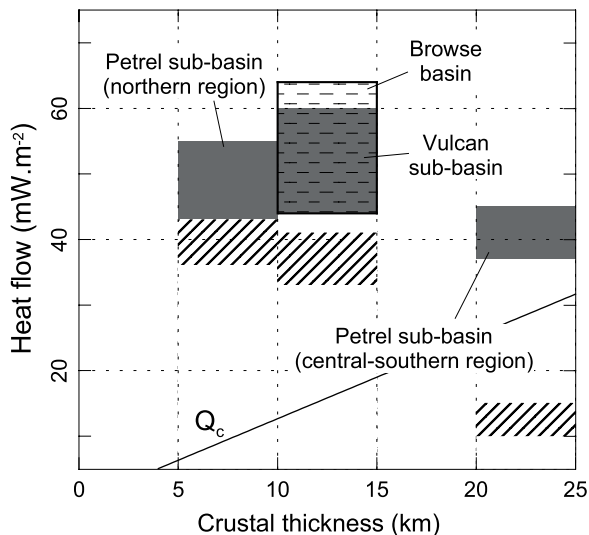


Figure 10. Heat flow corrected for the sediment contributions versus crustal thickness in the Browse, Vulcan, and Petrel basins (northwestern margin). Solid line: estimate of the crustal contribution Q_c (see text for details). Hatched areas: estimated range for mantle heat flow.

with experiments and numerical simulations of fluid convection involving an insulating lid, which show that heat flow increases at the border of the lid [Guillou and Jaupart, 1995; Grigné and Labrosse, 2001]. However, these studies model the continent as a different boundary condition on top of the convecting fluid, and predict an extremely high anomaly at the border of the continent, which is certainly the consequence of unrealistically high horizontal thermal gradients generated at the abrupt transition between the continent- and ocean-type boundary condition. More realistic simulations entailing deep continental roots within the convection system suggest that changes in the lithosphere thickness can generate small-scale instabilities [King and Anderson, 1998; O'Neill et al., 2003]. Therefore it would be worth to place continental margins at the scale of mantle convection and carry out similar simulations in order to quantify the convecting structures and the thermal regime at the border of continental roots.

Acknowledgments

[34] Wiltshire Geological Services[®] provided us the vast set of oil exploration data used in this study. D. Chapman and an anonymous reviewer helped to clarify the first version of this article. This is IGP contribution 2347.

References

- AGSO North West Shelf Study Group (1994), Deep reflections on the North West Shelf: Changing perceptions of basin formation, in *The Sedimentary Basins of Western Australia: Proceedings of the Petroleum Exploration Society of Australia Symposium, Perth, WA*, edited by P. G. Purcell and R. R. Purcell, pp. 63–76, Pet. Explor. Soc. of Aust., West Perth, Australia.
- Armstrong, P., R. Allis, R. Funnell, and D. Chapman (1998), Late Neogene exhumation patterns in Taranaki Basin (New Zealand): Evidence from offset porosity-depth trends, *J. Geophys. Res.*, *103*(B12), 30,269–30,282, doi:10.1029/98JB02843.
- Baldwin, S., N. White, and R. Müller (2003), Resolving multiple rift phases by strain-rate inversion in the Petrel Sub-basin, northwest Australia, *Spec. Pap. Geol. Soc. Am.*, *372*, 245–263. (Also *Spec. Publ. Geol. Soc. Aust.*, *22*, 245–263.)
- Ballard, S., and H. Pollack (1987), Diversion of heat by Archean cratons: A model for Southern Africa, *Earth Planet. Sci. Lett.*, *85*, 253–264.
- Bodorkos, S., M. Sandiford, B. Minty, and R. Blewett (2004), A high-resolution, calibrated airborne radiometric dataset applied to the estimation of crustal heat production in the Archean northern Pilbara Craton, Western Australia, *Precambrian Res.*, *128*, 57–82.
- Bücker, C., and L. Rybach (1996), A simple method to determine heat production from gamma-ray logs, *Mar. Pet. Geol.*, *13*(4), 373–375.
- Bullard, E. (1947), The time taken for a borehole to attain temperature equilibrium, *Mon. Not. R. Astron. Soc.*, geophys. suppl., *5*, 127–130.
- Chapman, D., T. Kehe, and M. Picard (1984), Heat flow in the Uinta basin determined from bottom hole temperature (BHT) data, *Geophysics*, *49*, 453–466.
- Cull, J. (1982), An appraisal of Australian heat flow data, *BMR J. Aust. Geol. Geophys.*, *7*, 11–21.
- Deming, D., and D. Chapman (1988), Heat flow in the Utah-Wyoming thrust belt from analysis of bottom-hole temperature data measured in oil and gas wells, *J. Geophys. Res.*, *93*(B11), 13,657–13,672.
- Driscoll, N., and G. Karner (1998), Lower crustal extension across the Northern Carnarvon basin, Australia: Evidence for an eastward dipping detachment, *J. Geophys. Res.*, *103*(B3), 4975–4991.
- Finlayson, D., C. Collins, I. Lukaszczuk, and E. Chudyk (1998), A transect across Australia's southern margin in the Otway Basin region: Crustal architecture and the nature of rifting from wide-angle seismic profiling, *Tectonophysics*, *288*, 177–189.
- Funnell, R., D. Chapman, R. Allis, and P. Armstrong (1996), Thermal state of the Taranaki Basin, New Zealand, *J. Geophys. Res.*, *101*(B11), 25,197–25,215.
- Goncharov, A. (2004), Basement and crustal structure of the Bonaparte and Browse basins, Australian northwest margin, in *Timor Sea Petroleum Geoscience, Proceedings of the Timor Sea Symposium, Darwin, Northern Territory, 19–20 June 2003, Spec. Publ. 1*, edited by G. Ellis, P. Baillie, and T. Munson, Northern Territory Geol. Surv., Darwin, Australia.
- Goutorbe, B., F. Lucazeau, and A. Bonneville (2006), Using neural networks to predict thermal conductivity from geophysical well logs, *Geophys. J. Int.*, *166*, 115–125, doi:10.1111/j.1365-246X.2006.02924.x.
- Goutorbe, B., F. Lucazeau, and A. Bonneville (2007a), Comparison of several BHT correction methods: A case study on an Australian data set, *Geophys. J. Int.*, *170*, 913–922, doi:10.1111/j.1365-246X.2007.03403.x.
- Goutorbe, B., F. Lucazeau, and A. Bonneville (2007b), The thermal regime of South African continental margins, *Earth Planet. Sci. Lett.*, *267*, 256–265, doi:10.1016/j.epsl.2007.11.044.
- Grigné, C., and S. Labrosse (2001), Effects of continents on Earth cooling: Thermal blanketing and depletion in radioactive elements, *Geophys. Res. Lett.*, *28*(14), 2707–2710.
- Guillou, L., and C. Jaupart (1995), On the effect of continents on mantle convection, *J. Geophys. Res.*, *100*(B12), 24,217–24,238.
- Jaupart, C., and J. Mareschal (1999), The thermal structure and thickness of continental roots, *Lithos*, *48*, 93–114.
- Kaplan, A., C. Lusser, and I. Norton (1985), Tectonic map of the world, Exxon Res. Co., Houston, Tex.
- King, S., and D. Anderson (1998), Edge-driven convection, *Earth Planet. Sci. Lett.*, *160*, 289–296.
- Leemans, R., and W. Cramer (1991), The IIASA database for mean monthly values of temperature, precipitation and cloudiness of a global terrestrial grid, *Tech. Rep. RR-91-18*, Int. Inst. for Appl. Syst. Anal., Laxenburg, Austria.
- Levitus, S., and T. Boyer (1994), *World Ocean Atlas 1994*, vol. 4, *Temperature*, Natl. Environ. Satel. Data and Inf. Serv., Natl. Oceanic and Atmos. Admin., Silver Spring, Md.
- Lide, D. (2004), *CRC Handbook of Chemistry and Physics*, 85th ed., CRC Press, Boca Raton, Fla.
- Lucazeau, F., and S. Le Douaran (1985), The blanketing effect of sediments in basins formed by extension: A numerical model. Application to the Gulf of Lion and Viking Graben, *Earth Planet. Sci. Lett.*, *74*, 92–102.

- Lucazeau, F., F. Brigaud, and J. L. Bouroullec (2004), High-resolution heat flow density in the lower Congo basin, *Geochem. Geophys. Geosyst.*, 5, Q03001, doi:10.1029/2003GC000644.
- McKenzie, D. (1978), Some remarks on the development of sedimentary basins, *Earth Planet. Sci. Lett.*, 40, 25–32.
- Middleton, M. (1982), Bottom-hole temperature stabilization with continued circulation of drilling mud, *Geophysics*, 47(12), 1716–1723.
- Miller, J., M. Norvick, and C. Wilson (2002), Basement control on rifting and the associated formation of ocean transform faults — Cretaceous continental extension of the southern margin of Australia, *Tectonophysics*, 359, 131–155.
- Müller, D., W. Roest, J.-Y. Royer, L. Gahagan, and J. Sclater (1997), Digital isochrons of the world's ocean floor, *J. Geophys. Res.*, 102, 3211–3214.
- Neumann, N., M. Sandiford, and J. Foden (2000), Regional geochemistry and continental heat flow: Implications for the origin of the South Australian heat flow anomaly, *Earth Planet. Sci. Lett.*, 183, 107–120.
- Nyblade, A. (1997), Heat flow across the East African Plateau, *Geophys. Res. Lett.*, 24(16), 2083–2086.
- O'Neill, C., L. Moresi, A. Lenardic, and C. Cooper (2003), Inferences on Australia's heat flow and thermal structure from mantle convection modeling results, *Spec. Pap. Geol. Soc. Am.*, 372, 169–184. (Also *Spec. Publ. Geol. Soc. Aust.*, 22, 245–263.)
- Pandey, O. (1981), Terrestrial heat flow in New Zealand, Ph.D. thesis, 194 pp., Victoria Univ., Wellington, New Zealand.
- Perrier, J., and J. Raiga-Clemenceau (1984), Temperature measurements in boreholes, in *Thermal Phenomena in Sedimentary Basins*, edited by B. Durand, pp. 47–54, Ed. Technip, Paris.
- Petkovic, P., C. Collins, and D. Finlayson (2000), A crustal transect between Precambrian Australia and the Timor Trough across the Vulcan Sub-basin, *Tectonophysics*, 329, 23–38.
- Pollack, H., S. Hurter, and J. Johnson (1991), A new global heat flow compilation, Dep. of Geol. Sci., Univ. of Michigan Ann Arbor, Ann Arbor.
- Pribnow, D., M. Kinoshita, and C. Stein (2000), Thermal data collection and heat flow recalculations for ODP Legs 101–180, Inst. for Jt. Geosci. Res., GGA, Hannover, Germany. (Available at <http://www-odp.tamu.edu/publications/heatflow/>)
- Rudnick, R., and D. Fountain (1995), Nature and composition of the continental crust: A lower crustal perspective, *Rev. Geophys.*, 33, 267–309.
- Sass, J., and A. Lachenbruch (1979), Thermal regime of the Australian continental crust, in *The Earth — Its Origin, Structure and Evolution*, edited by M. W. McElhinny, pp. 301–351, Academic, London.
- Serra, O., and L. Serra (2004), *Well logging — Data Acquisition and Applications*, Serralog, Méry Corbon, France.
- Shapiro, N., and M. Ritzwoller (2004), Inferring surface heat flux distributions guided by a global seismic model: Particular application to Antarctica, *Earth Planet. Sci. Lett.*, 223, 213–224.
- Shaw, R., P. Wellman, P. Gunn, A. Whitaker, C. Tarlowski, and M. Morse (1996), Users guide to the Australia crustal elements map, *AGSO Rec. 1996/30*, Aust. Geol. Surv. Org., Canberra.
- Simons, F., A. Zielhuis, and R. van der Hilst (1999), The deep structure of the Australian continent from surface wave tomography, *Lithos*, 48, 17–43.
- Song, T., and P. Cawood (2000), Structural styles in the Perth Basin associated with the Mesozoic break-up of Greater India and Australia, *Tectonophysics*, 317, 55–72.
- Studt, F., and G. Thompson (1969), Geothermal heat flow in the North Island of New Zealand, *N. Z. J. Geol. Geophys.*, 12, 673–683.
- Sutherland, F. (1978), Mesozoic-Cainozoic volcanism of Australia, *Tectonophysics*, 48, 413–427.
- Symonds, P., C. Collins, and J. Bradshaw (1994), Deep structure of the Browse basin: Implications for basin development and petroleum exploration, in *The Sedimentary Basins of Western Australia: Proceedings of the Petroleum Exploration Society of Australia Symposium, Perth, Western Australia*, edited by P. G. Purcell and R. R. Purcell, pp. 315–331, Pet. Explor. Soc. of Aust., West Perth, Australia.
- Vasseur, G., F. Lucazeau, and R. Bayer (1985), The problem of heat flow density determination from inaccurate data, *Tectonophysics*, 121, 25–34.
- Voorhoeve, H., and G. Houseman (1988), The thermal evolution of lithosphere extending on a low-angle detachment zone, *Basin Res.*, 1, 1–9.
- Vosteen, H., and R. Schellschmidt (2003), Influence of temperature on thermal conductivity, thermal capacity and thermal diffusivity for different types of rock, *Phys. Chem. Earth*, 28, 499–509.